Catalysis Letters Vol. 105, Nos. 1–2, November 2005 (© 2005)
DOI: 10.1007/s10562-005-8011-3

CO hydrogenation to light alkenes over Mn/Fe catalysts prepared by coprecipitation and sol-gel methods

Chong Wang, Qingxia Wang, Xinde Sun, and Longya Xu*

State Key Laboratory of Catalysis, Dalian Institute of Chemical Physics, Chinese Academy of Sciences, Dalian, P.O. Box 110, 116023, P.R. China

Received 30 January 2005; accepted 31 July 2005

CO hydrogenation to light alkenes was carried out on manganese promoted iron catalysts prepared by coprecipitation and sol-gel techniques. Addition of manganese in the range of 1–4 mol.% by means of coprecipitation could improve notably the percentage of $C_2^=$~$C_4^=$ in the products, but it was not so efficient when the sol-gel method was employed. XRD and H_2-TPR measurements showed that the catalyst samples giving high $C_2^=$~$C_4^=$ yields possessed ultrafine particles in the form of pure α-$(Fe_{1-x}Mn_x)_2O_3$, and high quality in lowering the reduction temperature of the iron oxide. Furthermore, these samples displayed deep extent of carburization and different surface procedures to the others in the tests of Temperature Programmed Surface Carburization (TPSC). The different surface procedures of these samples were considered to have close relationship with the evolving of surface oxygen. It was also suggested that for the catalysts with high $C_2^=$~$C_4^=$ yields, the turnover rate of the active site could be kept at a relatively high level due to the improved reducing and carburizing capabilities. Consequently, there would be a large number of sites for CO adsorption/dissociation and an enhanced carburization environment on the catalyst surface, so that the process of hydrogenation could be suppressed relatively to a low level. As a result, the percentage of the light alkenes in the products could be raised.

KEY WORDS: CO hydrogenation; light alkenes; manganese oxide; iron catalysts.

1. Introduction

Producing light alkenes via CO hydrogenation is one of the most promising processes for obtaining alkenes from non-petroleum based supply. However, low selectivity to the desired products ruled by the Anderson–Schulz–Flory (ASF) distribution function [1] has restricted the application of this process into an industrial scale. To surmount the effect of the ASF distribution, a great deal of research work has been carried out and some distinct improvements have been achieved [2]. Potassium and manganese oxides have been found to be the most efficient promoters among all the additives studied up to now.

As a conventional promoter, manganese has been widely used in many catalysts for Fischer–Tropsch synthesis (FTS) [3–6], and most researchers agreed that the addition of manganese could modify the iron catalysts to improve the selectivity of light alkenes in the products [7–10]. In our previous work [9], the promotion effect of manganese on the selectivity to light alkenes has been studied over impregnated iron catalysts supported on silicate-2, and it was found that the manganese could prohibit the secondary hydrogenation of C_2H_4 and C_3H_6.

There are also some results [11,12] indicating that the iron based catalysts with different manganese contents showed no relationship between the alkenes selectivity and the amount of manganese oxide added. We are interested in putting this topic into discussion because our experimental results showed that introducing manganese oxide into the iron catalysts with different method could result in different effect on the CO hydrogenation as the selectivity of light alkenes was considered.

Recently, detailed studies on the structure and the evolution of the iron catalysts on active surface indicated that the working surface in F–T synthesis might be described as a dynamic phase, surrounding a thermodynamically stable oxide or carbide core, and consisting of oxygen and carbon vacancies, surface oxygen, and carbon atoms occupying lattice positions in the underlying bulk [13–15]. Through the study on the carburizing performance of the unreduced K/Cu/Fe catalysts, Li *et al.* [15] have proved that the presence of K and Cu increased the F–T rates as well as the extent of steady-state carburization by providing nucleation sites for the formation of smaller FeC_x crystallites. These smaller active domains can lead, in turn, to shorter diffusion paths and larger number of sites for CO adsorption/dissociation and for FTS. In this work, carburization performances were investigated on reduced Mn/Fe catalysts, and some novel phenomena were reported.

2. Experimental

2.1. Catalyst preparation

Two methods were adopted in the preparation process: coprecipitation and sol-gel. Samples with different

* To whom correspondence should be addressed.
E-mail: lyxu@dicp.ac.cn

atomic ratio of manganese to iron were listed in table 1. In the coprecipitation method, catalysts were prepared from solutions of metal nitrates of $Fe(NO_3)_3{\cdot}9H_2O$ and $Mn(NO_3)_2$, and aqueous ammonia was used as the precipitating agent. The precipitates were washed with distilled water and dried at 120 °C before calcination.

Preparation using the sol-gel method was operated as described in reference [16]. Citric acid was added slowly into a mixed aqueous solution of $Fe(NO_3)_3$ and $Mn(NO_3)_2$ with different ratio of Mn/Fe under constant stirring. After that, the mixture was kept in a water bath at 60 °C until the solution became gelatinous, and then it was dried at 120 °C for 24 h. All final catalysts were calcined in air at 300 °C, and then at 500 °C for 2 h, respectively.

2.2. Catalyst characterization

X-ray diffraction patterns were recorded on a Rigaku D/MAX-RB instrument with Cu$K_{\alpha 1}$ radiation (λ = 1.54 Å), 2θ starting from 10° to 70°, at 40 kV, 50 mA. The morphology of the catalysts was studied by TEM on a JEOL JEM-1200EX.

For H_2-TPR measurements, samples of 50 mg were loaded in a U-type quartz tube and kept at 120 °C for 60 min in flowing Ar. After the temperature had dropped to the ambient temperature, a flow of 10 vol.% H_2 in Ar was introduced at 20 mL/min. The TPR procedure was started from ambient temperature to 800°C at a constant heating rate of 10 °C/min, and the temperature was held at 800 °C until no more H_2 consumption was detected. The amount of H_2 in the gas flow was monitored by a TCD.

The BET surface areas of the samples were determined from the isotherms of nitrogen physisorption on a NOVA 4000 gas adsorption analyzer. Each sample was degassed at 350 °C for 2 h before the tests.

Carburization of the reduced samples was measured by a technique of Temperature Programmed Surface Carburization (TPSC), using CO as the carburizing agents. The sample (0.1 g, 100–120 μm) was placed in a U-type quartz tube and reduced in H_2 (50 mL/min) at 450 °C for 2 h. After the sample was cooled to ambient temperature in Ar, the stream was switched to a flow of CO in Ar (CO/Ar = 20/80 kPa) with a total flow rate of 50 mL/min. Then the temperature was increased up to the target value at a rate of 10 °C/min. A part of the effluent stream was diverted into a differentially pumped atmospheric sampling system connected to a quadrupole mass spectrometer (Ominstar 300).

The H_2/CO-TPSR (Temperature Programmed Surface Reaction) was carried out under similar conditions to those of the CO-TPSC, only with syngas in Ar (H_2/CO/Ar = 40/20/40 kPa) substituting for CO/Ar.

2.3. Catalytic tests

Catalytic tests of CO hydrogenation were performed in a stainless steel fixed-bed reactor. The catalysts were sieved into 20–40-mesh particles. Samples of 2 mL were loaded in an 8-mm-i.d. tube, where prereduction was undertaken at 450 °C for 2 h in a pure H_2 flow at 2 L/h. Then the reaction was carried out at 350 °C, 1.5 MPa syngas (H_2/CO = 2), and 1000 h^{-1}. The tail gas was analyzed by an on-line gas chromatograph equipped with TCD.

3. Results

3.1. Performance in CO hydrogenation

Reaction data of CO hydrogenation collected after 300 min time on stream (TOS) are arranged in table 2. It can be seen that for CO conversion, both the coprecipitated and the sol-gel prepared samples with low manganese contents (not higher than 4 mol.%) give CO conversion higher than 90%. However, as the amount of the added manganese was increased, the CO conversion declined.

Catalysts prepared by coprecipitation and sol-gel show quite different behaviors for light alkenes selectivity. It is quite notable that there is no ethene in the products of CP-0 and all the catalysts prepared by sol-gel method. The very low ethene yield has also been reported [17], and no ethene was found in the products on a Mn/Fe (Mn/Fe = 4 atomic ratio) sample [18]. However, no special explanation was given for these phenomena in the literature. We have tried to give a tentative explanation for the absence of ethene in the products of our sol-gel prepared samples as well as CP-0. However, the virtual reasons are still unknown up to now.

On the other hand, significant amount of ethene appeared over the Mn-promoted samples (CP-1, CP-2 and CP-3) prepared by coprecipitation. In addition, the percentage of C_3^0 declined greatly in these samples,

Table 1
BET specific surface area of Mn/Fe catalysts prepared with different methods

Preparing method	Coprecipitation					Sol-gel				
Sample	CP-0	CP-1	CP-2	CP-3	CP-4	SG-0	SG-1	SG-2	SG-3	SG-4
Mn:Fe (atomic)	0:100	1:99	4:96	15:85	25:75	0:100	1:99	4:96	15:85	25:75
Surface area (m^2/g)	20.4	12.6	10.7	35.1	49.8	4.8	3.2	3.3	5.9	14.3

Table 2
Catalytic performance in CO hydrogenation

Sample	CO conversion (%)	Distributions of the hydrocarbons in the products (wt.%)					
		CH_4	$C_2^=$	C_2^0	$C_3^=$	C_3^0	$C_2^=\sim C_4^=$
CP-0	91.8	36.7	0	19.4	16.4	14.9	26.0
CP-1	94.0	27.9	11.3	10.8	20.5	4.8	51.3
CP-2	96.3	29.7	11.7	11.5	20.6	4.8	52.1
CP-3	85.2	32.0	12.7	19.5	19.7	3.9	43.6
CP-4	77.8	36.5	4.6	18.6	14.9	11.3	28.3
SG-0	91.6	38.4	0	16.9	7.6	19.1	18.0
SG-1	95.5	37.8	0	17.6	7.7	19.2	19.2
SG-2	90.2	36.0	0	15.3	14.7	12.9	31.2
SG-3	73.9	32.1	0	19.7	11.6	16.8	23.7
SG-4	61.9	44.3	0	19.2	4.6	19.7	9.8

Reaction condition: 350 °C, 1.5 MPa, 1000 h^{-1}, H_2/CO = 2 (V/V), TOS = 300 min.

which in turn resulted in the increase of the ratio of $C_3^=/C_3^0$ evidently. In detail, as 1 mol.% of Mn was added by coprecipitation, the percentage of $C_2^=\sim C_4^=$ was promoted greatly from 26.0 wt.% (CP-0) up to 51.3 wt.% (CP-1). When the ratio of Mn/Fe was 4/96 (CP-2), the $C_2^=\sim C_4^=$ content reached a maximum (52.1 wt.%, table 2).

For the samples prepared by sol-gel method, the percentage of the light alkenes from C2 to C4 was also increased after the addition of the manganese. However this increase is not as evident as in the coprecipitated samples. It can be found that the percentage of $C_2^=\sim C_4^=$ was 19.2 over SG-1, which was only 1.2 points higher than that on SG-0. Although sample SG-2 showed the highest percentage of $C_2^=\sim C_4^=$ (31.2 wt.%), yet it was much smaller than that on CP-2.

Further increase of manganese content either by coprecipitation or by sol-gel method brought about decreases both in CO conversion and the percentage of $C_2^=\sim C_4^=$. It can be seen from table 2 that for CP-4, CO conversion is 77.8% and the percentage of $C_2^=\sim C_4^=$ has dropped to 28.3 wt.%. As for SG-4, the two corresponding values are 61.9% and 9.8 wt.%, respectively.

The impact of the preparation methods on the stability of the catalysts was investigated on the samples of CP-2 and SG-2. It can be seen from figure 1 that the CO conversion of both catalysts decreased to ca. 67% at a TOS of 24 h. The amount of methane in the hydrocarbons remained in relatively steady values, i.e. 29.8 wt.% for CP-2 and 36.4 wt.% for SG-2. After 24 h of reaction, for SG-2 the percentage of $C_2^=\sim C_4^=$ increased from initial 25.7 up to 48.4 wt.%, while for CP-2 the variation was not notable.

According to the above results, we can conclude that the preparation methods of the Mn/Fe catalysts have obvious influence on the products distribution in CO hydrogenation. However, with respect to the impact on the catalytic activity, the difference between these two preparation methods is limited.

3.2. Characters of the microstructure

XRD patterns of the samples with different atomic ratios of Mn/Fe after calcination are displayed in figure 2. The structure of hematite (α-Fe_2O_3) is evident for the samples of CP-0 and SG-0. For the other samples with addition of manganese, the XRD patterns are almost the same as that of the pure iron samples, except that the intensities of the diffraction peaks are different.

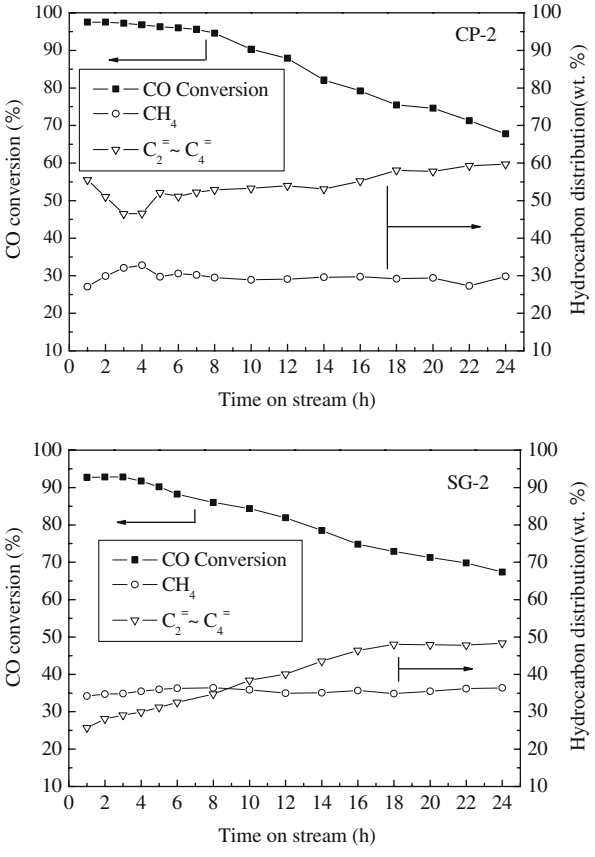

Figure 1. CO hydrogenation performance of sample CP-2 (above) and SG-2 (below) within 24 h.

According to the results in the literature [18,19], after calcination at 500 °C, the Fe-rich catalysts would exist in the single solid solution phase of Mn in hematite, hence the other samples in figure 2 could be designated as α-$(Fe_{1-x}Mn_x)_2O_3$. At the same manganese content, the diffraction peaks of the samples prepared by sol-gel are much higher than those coprecipitated samples, which indicate that the coprecipitated samples are in a state of higher dispersion than the sol-gel prepared ones. In accordance with the XRD analysis, the results of the BET surface area in table 1 also provide some evidence standing for this speculation, since the coprecipitated samples possessed larger surface area than the sol-gel prepared ones at the same manganese content.

As for the samples of high manganese contents, such as CP-4 and SG-4, the massively introduced manganese oxide had brought about remarkable impact on the XRD diffraction patterns. As can be seen in figure 2, the intensity of the diffraction peaks of CP-4 and SG-4 decreases greatly in comparison with those of the pure Fe sample. The morphology of the samples with high manganese contents were different from those of the samples with low Mn contents, which has been identified by TEM. For instance, it can be seen from the TEM image in figure 3 (right) that there are some long and narrow cubic crystals in sample CP-4, which were attributed to cubic Mn_2O_3 [20] or cubic $(Mn, Fe)_2O_3$ [18]. Figure 3 (left) shows the TEM result of sample CP-2, in which no cubic crystal can be found. The appearance of these cubic crystals indicates that at high concentration, the additional manganese oxides, which can not be accommodated within the solid solution of α-$(Fe_{1-x}Mn_x)_2O_3$, will exist in a separated phase of cubic structure. The reason that this phase does not appear in the XRD spectra might be due to the low concentration or the weak diffraction intensity of the cubic crystal itself.

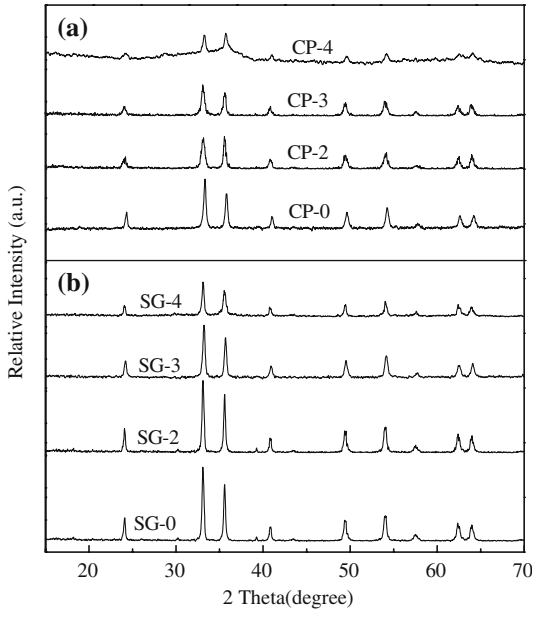

Figure 2. XRD diffraction spectra of Mn/Fe catalysts prepared by coprecipitaion (a) and sol-gel method (b).

3.3. Comparison of the reducibility

H_2-TPR profiles of the samples prepared by coprecipitation and sol-gel methods are displayed in figure 4. For the pure iron samples of CP-0 and SG-0, the three hydrogen consumption peaks of I (represents the first initial reduction peak), M (represents the second peak in the medium temperature range) and H (the last peak in the region of high temperature) could be considered as the reduction from Fe_2O_3 to Fe_3O_4 [21,22], from Fe_3O_4 to FeO and from FeO to Fe [20], respectively. In the case of small manganese amount (below 4 mol.%) added by means of coprecipitation, the whole H_2-TPR profiles shift to the low temperature field. For peak I, this shift is about 70 °C, while for peak M it is ca. 50 °C. Although, for the samples prepared by sol-gel method, the addition of manganese oxides as well lowered the reduction temperature, the shift is not as remarkable as in the coprecipitated samples.

As the manganese content was higher than 15 mol.%, a new reducing peak below 400 °C appeared in the H_2-TPR profiles. Comparing with the H_2-TPR profiles of the pure manganese samples in figure 4, this TPR peak might be attributed to the reduction from Mn_2O_3 to Mn_3O_4 [23]. The appearance of this peak gives another credible proof of the existence of the cubic phase in the samples with high manganese contents. This peak can be seen clearly in the profile of sample CP-4, while in profiles CP-3, SG-3 and SG-4, it is not so evident, possibly due to the poor concentration of Mn_2O_3 in the sample, as compared to the phase of α-$(Fe_{1-x}Mn_x)_2O_3$.

3.4. Carburization results in CO-TPSC tests

Temperature Programmed Surface Carburization (TPSC) tests in CO atmosphere were carried out on the reduced samples in order to study the interactions between CO and metal atoms in different catalysts. This is different from the traditional CO-TPR (Temperature Programmed Reduction) studies, in which fresh catalyst oxides react with CO directly. In the pretreatment of CO-TPSC, the samples were reduced in H_2 (50 mL/min) at 450 °C for 2 h. XRD and H_2-TPR identified that the iron oxide in this case has been reduced to Fe^0. Hence in the subsequent TPSC tests, the carburizing process will start with metallic iron. It is known that carburization is a very complicated process, including adsorption/dissociation of the CO molecule, formation of iron carbides/oxide and some reactions even in the gas phase, such as the Boudouard reaction. (The details will be presented in the discussion section.) Some of these procedures do not have definite stoichiometry. For instance, in the formation of iron carbides, the structures of iron carbides are very complicate (at least five

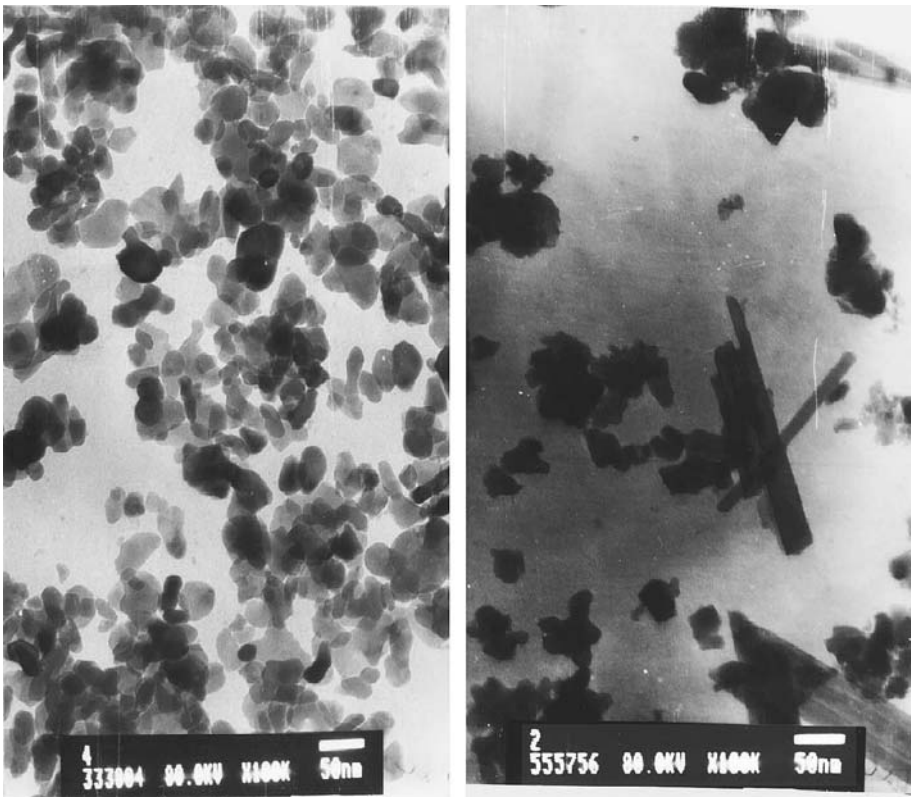

Figure 3. TEM images of the fresh sample of CP-2 (left) and CP-4 (right).

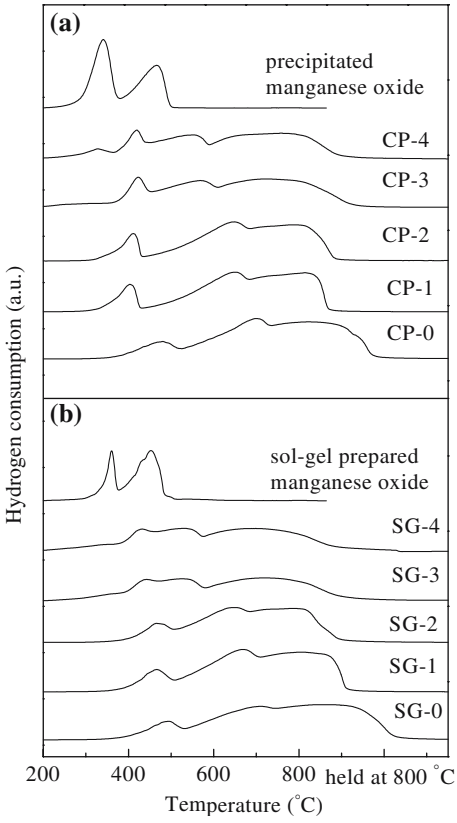

Figure 4. H_2-TPR profiles of the Mn/Fe catalysts prepared by coprecipitaion (a) and sol-gel method (b).

different forms of iron carbides are known to exist [24]), and in most cases, more than one iron carbide might form at the same time. Therefore, the quantification relationship between CO and the sample is really difficult to be described in the TPSC tests, and the following analysis will be based on comparisons of the relative ion currents detected by MS in the TPSC profiles of various samples.

Figure 5 presents the profiles of the ion currents of CO (a) and CO_2 (b) in the exit gas during the CO-TPSC. Comparing figure 5a, b, we can observe that CO consumption and CO_2 formation are almost in the same trend, which indicates that the above two procedures are linked together through a series of closely related surface courses.

In figure 5a, for the coprecipitated samples, there are three sets of CO consumption peaks, whose temperatures are centered at ca. 260, 390 and 550 °C, respectively. The area of the medium temperature (ca. 390 °C) peak is much smaller than those of the low (ca. 260 °C) and the high temperature (550 °C) peak.

As for the sol-gel prepared samples, however, only two CO consumption peaks appear in the profiles, with the medium temperature peak absent. With regard to the low temperature (260 °C) peak, the amount of CO consumption of the coprecipitated samples is much larger than those of the sol-gel prepared samples at the same Mn content. Moreover, this disparity becomes

more notable with the increase of the Mn content. Similar trend is exhibited in the profiles of CO_2 formation. From above results in CO-TPSC, it can be considered that the extent of the carburization on the coprecipitated samples is deeper than on those sol-gel prepared samples.

3.5. Results of syngas-TPSR

Substituting the CO/Ar flow by a mixed gas of $40H_2/20CO/40Ar$, we made a further investigation on the reduced samples in the syngas atmosphere. In figure 6a, three CO_2 formation peaks could also be distinguished for the coprecipitated samples, but they are not as obviously as in the CO-TPSC operations (figure 5) due to the overlapping of the last two peaks. The first peak is located in the low temperature zone centering at around 280 °C, and the other two peaks are at ca. 400 and 500 °C, respectively. It seems that the addition of manganese by means of coprecipitation does not alter the outlines of the peaks in the syngas-TPSR profiles, while for the sol-gel prepared samples, these CO_2 peaks are weakened as the manganese content is increased, until the first peak is significantly reduced for SG-4 with the highest loading of Mn. Therefore, it could be considered that with the addition of the manganese oxide and in the syngas atmosphere, the carburizing process is suppressed for the sol-gel prepared samples, which is consistent with the former results in CO-TPSC.

Figure 6b is the profiles of H_2O in syngas-TPSR. It is observed that the H_2O peak appears before CO_2. The reason might be that the H_2 is twice as much as CO in the feed, and hence within the initial stage of the syngas-TPSR, surface oxygen is more likely to combine with hydrogen to release H_2O, when the kinetic aspect is taken into account. It also can be found that with the proceeding of the TPSR, the slopes of the H_2O profiles in figure 6b does not change as much as the CO_2 profiles in figure 6a at temperatures below 350 °C. This indicates that, within this temperature range, as the temperature is increased, more surface oxygen will be removed by CO with the releasing of CO_2, which might be due to the reason that the formation of H_2O is not as favorable as that of CO_2 from thermodynamic considerations [25,26].

In the syngas-TPSR, the formation of CH_4 could reflect the amount of active carbonaceous species on the catalyst surface, because it is often used as a surrogate measuring of hydrocarbon synthesis rates [15]. In figure 6c, the CH_4 profiles display three peaks for the coprecipitated samples. As for the sol-gel prepared samples, the amount of CH_4 formation is less than that in the coprecipitated ones, which indicates that the amount of active carbonaceous species is higher on the surface of the coprecipitated Mn/Fe catalysts.

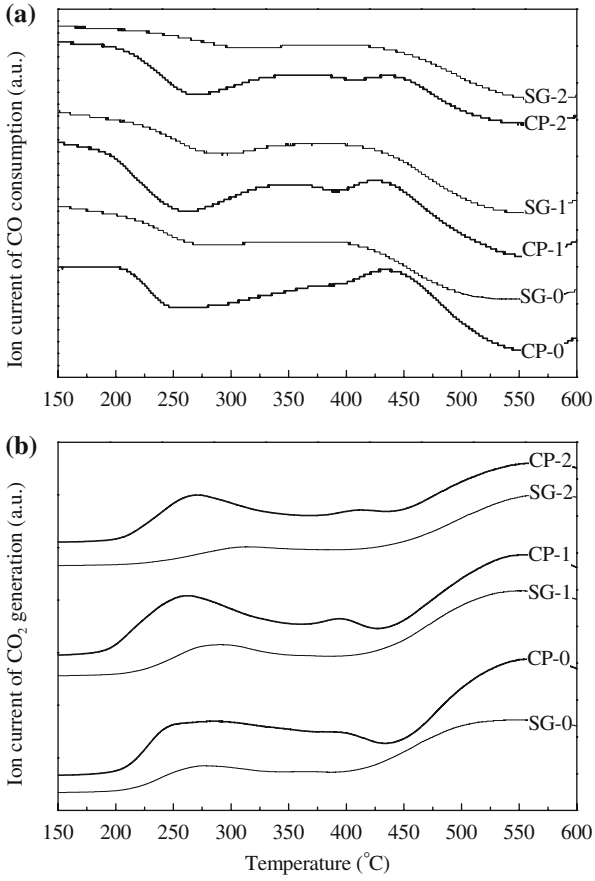

Figure 5. Ion current of CO (negative peaks) and CO_2 (positive peaks) detected by mass spectrometer in the tests of CO-TPSC.

4. Discussion

When in low contents, the added MnO could co-exist with iron atoms in the form of α-$(Fe_{1-x}Mn_x)_2O_3$. However, with the increase of the manganese content, there are some cubic structures formed in the catalysts as shown in the TEM image (figure 3-right). Meanwhile, both the CO conversion and the percentage of the light alkenes in the products decreased. All these results indicate that the cubic crystallites in the catalyst are detrimental to the conversion of syngas to light alkenes.

As for the samples with manganese content lower than 4 mol.%, most of the CO conversion reached more than 90%, no matter what kind of method was adopted in the preparation. However, the percentage of $C_2^{=}\sim C_4^{=}$ in the products showed much higher level for the coprecipitated samples than the ones prepared by sol-gel method. We will argue in detail about this difference between the two types of Mn/Fe catalysts prepared with different methods, taking CP-2 and SG-2 as examples.

The unpromoted samples CP-0 and SG-0 showed similar behavior in H_2-TPR tests, though CP-0 possessed larger BET surface than SG-0. This implies that in this present study the surface area does not have a

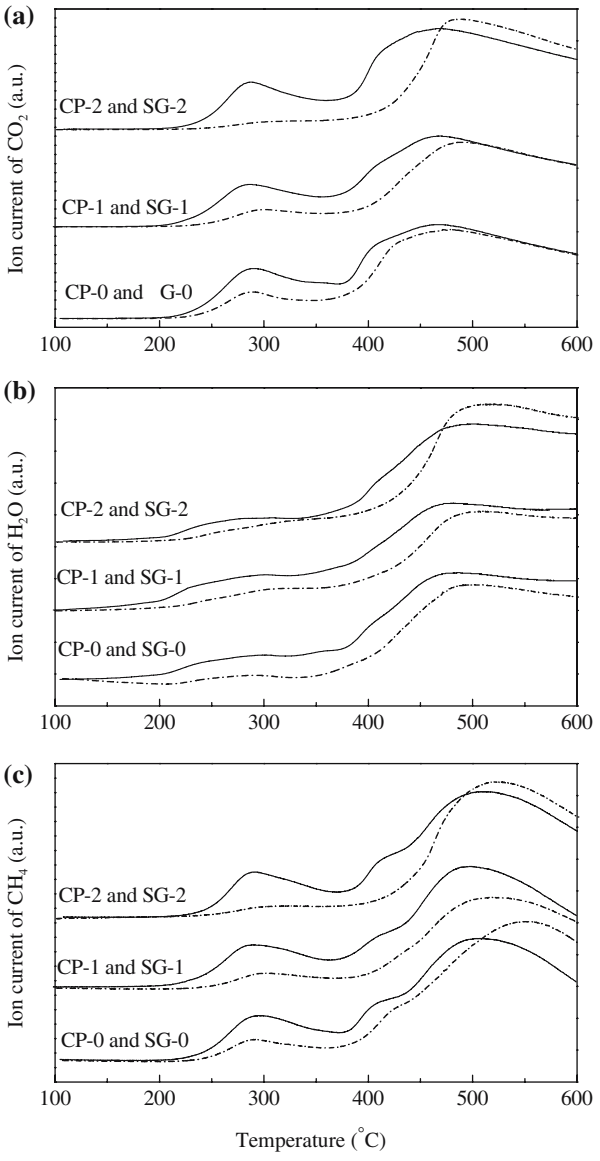

Figure 6. Ion current of CO_2 (a), H_2O (b) and CH_4 (c) detected by mass spectrometer in the tests of syngas-TPSR (solid lines for samples of CP series, dash dot lines for SG series).

direct impact on the H_2-TPR process. However, in a highly dispersed system with small particle size and large surface area, the added manganese could modify greatly the physico-chemical characteristics of the iron catalyst. It has been reported that manganese oxide could act as surface basicity as alkali metal does [27,28], or in other words, manganese oxide might act as a strong electron donor. This electron donating effect will in turn alter the biding energy [29]. Hence, it can be inferred that in a highly dispersed system (like in the case of CP-2), the basicity characteristic of Mn could function more efficiently. The H_2-TPR result that sample CP-2 showed superior capability to SG-2 in lowering the H_2-reducing temperature of the unpromoted iron catalyst might be related to the basicity of the manganese oxide.

The differences in particle size and H_2 reducibility led to the different performances between CP-2 and SG-2 in TPSC tests. In order to give a reasonable explanation for the discrepancy between them, all the possible surface courses should be taken into consideration. In the virtual F–T process, there exist many complicated transformations among diverse species in multiple forms on the active sites, some of which take place successively, while others occur in parallel ways. The evolution of the surface carbon species has been given a good annotation in the theory of competition [30,31]. As for the evolution of the dissociatively chemisorbed oxygen species, it has not been given as enough regards as for the surface carbon species. In this work, we found that only put the evolution of surface C and O species into a whole discussion could give a logical interpretation of the results in the TPSC tests. In figure 7, a modified model is proposed, in which the evolutions of surface C, O and H and the metal atom on the active site are illustrated in the same scheme.

In accordance with most of the other models, the whole procedure starts from the dissociation of the absorbed CO on the surface active sites, as shown in step 1 of figure 7. Hence, there exist two types of species on the active sites, i.e. surface C and O. According to the classical competition model [30], the competition of surface C includes steps 4, 7 and the formation of the unreactive graphitic-type carbon, i.e. the Boudouard reaction (not shown in figure 7). For the surface O species, there also exist some competitive courses similar to that of surface C. It is possible for the dissociated O species to either combine with H atoms to form water (as in step 8), or to react with CO to release CO_2 (as in step 5), through which the vacant active sites will be reproduced.

In the traditional mechanism of surface species [32], the discussion about the O species will be ended here. However, we consider that the O species could also migrate from upon the surface into the crystal lattice in the near surface layers of the catalysts, so that the metal atoms on the active sites transform into oxide form of $M_\beta O$ (step 2). In other words, step 2 is a reoxidation procedure of the metal on the active sites. Here, $M_\beta O$ is not considered as the dissociated adsorbed oxygen species, but as the precursor of some stable oxide forms like FeO or Fe_3O_4, which always exist in the used catalysts. In an oxidizing atmosphere, $M_\beta O$ could further be transformed into a more stable phase of $M_\lambda O$. On the other hand, in a reducing atmosphere, $M_\beta O$ could be reduced into metal phase M by CO through path 3 or by hydrogen in step 9. Consequently, the oxidized active sites are regenerated.

Through the description of this model above, it can be seen that for the surface C and O species there are several different procedures competing with each other. As for the iron metal atoms on the active sites, there are also various forms transforming from each other instanta-

neously. In the work of [15], the authors proposed that it is inaccurate and possibly misleading to describe Fe carbides or oxides as the active phases in FTS, because their interconversion occurs in the time scale of a reaction turnover. Therefore, here in our model of the surface processes, the definite assignments for the forms of M, $M_\alpha C$, $M_\beta O$ and $M_\lambda O$ were not given.

It has been observed that there are three CO consumption peaks in the CO-TPSC profiles of the coprecipitated sample CP-2, while in the sol-gel prepared sample SG-2, the mid peak (peak temperature at ca. 390 °C) is absent. According to the previous study of CO adsorption on Fe foil [33], the first CO consuming and CO_2 forming peak within the low temperature region are assigned to the procedures of steps 1 + 5, in which CO decomposes on the active sites and then the dissociatively chemisorbed O species combine with CO to form CO_2 in succession. As for the last CO consuming and CO_2 forming peaks in the high temperature zone, the Boudouard reaction itself ($2CO \rightarrow C + CO_2$), can give a good explanation for them. Therefore, referring back to the scheme of figure 7, the mid peak in CO-TPSC could be attributed to the course of step 3. In this step, the oxygen atom in $M_\beta O$ is removed by CO, with the regeneration of M and the release of CO_2.

It was pointed out that the reduction and the carburization of transition metal oxides are limited by the diffusion of the oxygen in the bulk lattice [14,34]. Because the coprecipitated samples possessed ultrafine particle as well as have more even distribution than the sol-gel prepared ones, the oxygen atoms in CP-2 can migrate in the near surface layers with less resistance. This is might be the reason that sample CP-2 is easier to be deoxidized in H_2-TPR and carburized during the CO-TPSC, as compared with SG-2. In turn, after the dissociatively adsorbed O atoms diffuse into the crystal lattice transforming into some transient intermediate such as $M_\beta O$ in step 2, the O atoms in the near surface layers of CP-2 might be eliminated by CO or H as in the manner of step 3 or 9, while for SG-2 this process would be retarded, especially in the case that CO is the reductant in the CO-TPSC. As a result, CP-2 can display the mid CO consumption peak in the CO-TPSC profiles, while SG-2 cannot. For the same reason, similar phenomena existed in the samples CP-1 and SG-1 as well.

On the other hand, the replacement of syngas as the carburizing agent in the syngas-TPSR makes the surface process more complicated. The profiles in the syngas-TPSR are not as explicit as in the CO-TPSC. However, from the relative intensities of the CO_2 and H_2O profiles in figure 6, we can observe more apparently the process of carburization in the samples prepared by coprecipitation. In addition, the triple-peak pattern in the CH_4 profile indicates that there is a higher amount of active C species on the surface of the coprecipitated samples.

Based on the analysis above, it can be visualized that there are larger numbers of sites for CO adsorption/dissociation on the Mn-modified coprecipitated samples than on the sol-gel prepared ones. As a result, the extent of carburization is stronger on the surface of the coprecipitated Mn/Fe catalysts. From another aspect, the additional surface course of step 3; in figure 7 allows the C species to have a longer life on the working surface of CP-2, which could also increase the extent of catalyst carburization [2]. For all the reasons mentioned above, there would exist on the working surface of CP-2 a relatively better environment of carburization in comparison with the environment for hydrogenation. Consequently, the rate of the secondary hydrogenation of the unsaturated hydrocarbons to alkanes is lowered, so that the percentage of $C_2^= \sim C_4^=$ is higher than that on SG-2.

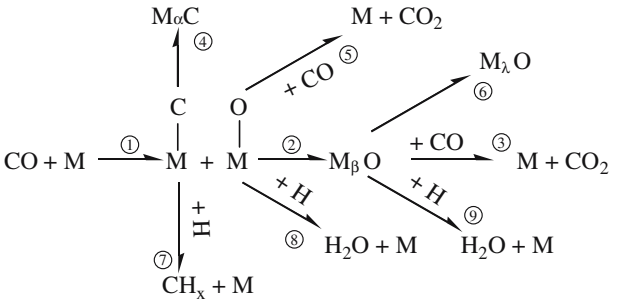

Figure 7. Evolution of the species on the active surface (M represents the metal atoms).

5. Conclusions

In this work, we prepared a series of Mn/Fe catalysts with different manganese contents both by coprecipitation and sol-gel methods. During CO hydrogenation tests, it was found that introducing manganese by coprecipitation increased twofold the percentage of $C_2^= \sim C_4^=$ in the products, while this promotion effect was not so remarkable on the sol-gel prepared Mn/Fe catalysts.

Physico-chemical analysis showed that samples with high yield of light alkenes have better reduction and carburization properties due to the modification of adding manganese by coprecipitation, which facilitates the oxidized active sites to be regenerated in the syngas atmosphere. This in turn can allow the catalyst surface to have a sufficient amount of active sites to adsorb and decompose CO. Therefore, the carburization environment on the surface is relatively improved and the rate of hydrogenation is relatively suppressed, which as a whole results in the high yield of light alkenes.

References

[1] P.J. Flory, J. Am. Chem. Soc. 58 (1936) 1877.
[2] R. Snel, Catal. Rev. Sci. Eng. 29 (1987) 361.
[3] B. Bussemeier, C.C. Frohning and B. Cornils, Hydrocarbon Process 55(11) (1976) 101.

[4] M. Janardanarao, Ind. Eng. Chem. Res. 29 (1990) 1735.
[5] D. Das, G. Ravichandran and D.K. Chakrabarty, Catal. Today 36 (1997) 285.
[6] U. Lüchner, H. Papp and M. Baerns, Appl. Catal. 23 (1986) 339.
[7] J. Barrault, C. Forquy and V. Perrichon, Appl. Catal. 5 (1983) 119.
[8] R. Malessa and M. Baerns, Ind. Eng. Chem. Res. 27 (1988) 279.
[9] L.Y. Xu, Q.X. Wang, Y.D. Xu and J.S. Huang, Catal. Lett. 31 (1995) 253.
[10] J. Venter, M. Kaminsky, G.L. Geoffroy and M.A. Vannice, J. Catal. 105 (1987) 155.
[11] W.L. van Dijk, J.W. Niemantsverdriet, A.M. van der Kraan and H.S. van der Baan, Appl. Catal. 2 (1982) 273.
[12] C.N. Satterfield and H.G. Stenger, Ind. Eng. Chem. Process Des. Dev. 23 (1984) 26.
[13] S. Li, R.J. O'Brien, G.D. Meitzner, H. Hamdehd, B.H. Davis and E. Iglesia, Appl. Catal. A 219 (2001) 215.
[14] S. Li, G.D. Meitzner and E. Iglesia, J. Phys. Chem. B 105 (2001) 5743.
[15] S. Li, W. Ding, G.D. Meitzner and E. Iglesia, J. Phys. Chem. B 106 (2002) 85.
[16] W.X. Kuang, Y.N. Fan and Y. Chen, J. Colloid Interface Sci. 215 (1999) 364.
[17] L.G. Alfonso, F. Bernardo, R. Fulgencio, M. Juan C. Rodrigo, Appl. Catal. A 177 (1999) 193.
[18] G.C. Maiti, R. Malessa, U. Lüchner, H. Papp and M. Baerns, Appl. Catal. 16 (1985) 215.
[19] N.K. Jaggi, L.H. Schwartz, J.B. Butt, H. Papp and M. Baerns, Appl. Catal. 13 (1985) 347.
[20] G.C. Maiti, R. Malessa and M. Baerns, Appl. Catal. 5 (1983) 151.
[21] T. Grzybek, H. Papp and M. Baerns, Appl. Catal. 29 (1987) 335.
[22] I.R. Leith and M.G. Howden, Appl. Catal. 37 (1988) 75.
[23] E.R. Stobbe, B.A. de Boer and J.W. Geus, Catal. Today 47 (1999) 161.
[24] J. Heon and J.T. William, J. Catal. 134 (1992) 654.
[25] A.G. Sault and A.K. Datye, J. Catal. 140 (1993) 136.
[26] D.B. Bukur, K. Okabe, M.P. Rosynek, C.P. Li, D.J. Wang, K.R.P.M. Rao and G.P. Huffman, J. Catal. 155 (1995) 353.
[27] M.E. Dry and G.J. Oosthuizen, J. Catal. 11 (1968) 18.
[28] K.B. Jensen and F.E. Massoth, J. Catal. 92 (1985) 98.
[29] G. Broyden, T.N. Rhodin, D.F. Brucker, R. Benbow and Z. Hurych, Surf. Sci. 59 (1976) 593.
[30] J.W. Niemantsverdriet, A.M. van der Kraan, W.L. van DiJk and H.S. van der Baan, J. Phys. Chem. 84 (1980) 3363.
[31] J.W. Niemantsverdriet and A.M. van der Kraan, J. Catal. 72 (1981) 385.
[32] D.J. Dwyer and J.H. Hardenbergh, J. Catal. 87 (1984) 66.
[33] H.P. Bonzel and H.J. Krebs, Surf. Sci. 117 (1982) 639.
[34] R. Kapoor and S.T. Oyama, J. Mater. Res. 12(2) (1997) 467.